

Claudin-2, a component of the tight junction, forms a paracellular water channel

Rita Rosenthal¹, Susanne Milatz¹, Susanne M. Krug¹, Beibei Oelrich¹, Jörg-Dieter Schulzke², Salah Amasheh¹, Dorothee Günzel¹ and Michael Fromm^{1,*}

¹Institute of Clinical Physiology and ²Department of General Medicine, Charité, Campus Benjamin Franklin, Freie Universität and Humboldt-Universität, 12200 Berlin, Germany

*Author for correspondence (michael.fromm@charite.de)

Accepted 22 March 2010
Journal of Cell Science 123, 1913–1921
 © 2010. Published by The Company of Biologists Ltd
 doi:10.1242/jcs.060665

Summary

Whether or not significant amounts of water pass the tight junction (TJ) of leaky epithelia is still unresolved, because it is difficult to separate transcellular water flux from TJ-controlled paracellular water flux. Using an approach without differentiating technically between the transcellular and paracellular route, we measured transepithelial water flux with and without selective molecular perturbation of the TJ to unequivocally attribute changes to the paracellular pathway. To this end, MDCK C7 cells were stably transfected with either claudin-2 or claudin-10b, two paracellular cation-channel-forming TJ proteins that are not endogenously expressed in this cell line. Claudin-2 is typical of leaky, water-transporting epithelia, such as the kidney proximal tubule, whereas claudin-10b is present in numerous epithelia, including water-impermeable segments of the loop of Henle. Neither transfection altered the expression of endogenous claudins or aquaporins. Water flux was induced by an osmotic gradient, a Na⁺ gradient or both. Under all conditions, water flux in claudin-2-transfected cells was elevated compared with vector controls, indicating claudin-2-mediated paracellular water permeability. Na⁺-driven water transport in the absence of an osmotic gradient indicates a single-file mechanism. By contrast, claudin-10b transfection did not alter water flux. We conclude that claudin-2, but not claudin-10b, forms a paracellular water channel and thus mediates paracellular water transport in leaky epithelia.

Key words: Epithelial water transport, Tight junction, Claudin-2, Claudin-10b, Paracellular channel

Introduction

Leaky epithelia such as the kidney proximal tubule and small intestine are characterized by high transport rates of ions and water. Although it has been established for several years that ions pass these epithelia by means of transcellular as well as paracellular pathways, the routes taken by water are still under controversial discussion. Since the discovery of aquaporin (AQP) water channels in both epithelial cell membranes, the molecular basis of a transcellular pathway has been evident (Agre et al., 1993). By contrast, the contribution of the paracellular pathway through the tight junctions (TJ) was estimated to be between 0 and 100%, depending on the method used for analysis (Kovbasnjuk et al., 1998; Quigley and Baum, 2002; Shachar-Hill and Hill, 2002; Spring, 1998; Zeuthen, 1995). Although TJs are often named aqueous pores, there is, as yet, no direct experimental evidence of paracellular water flux.

Technically, the obvious approach for the analysis of paracellular water flux would be to measure the rate of transepithelial water flux before and after blocking the TJ pathway. However, this approach has proven unsuccessful because transcellular side effects of paracellular permeability inhibitors could not be excluded (Loeschke and Bentzel, 1994; Poler and Reuss, 1987). The converse approach, blocking the transcellular water channels and measuring the resulting decrease in transepithelial water flux (Carpi-Medina and Whitembury, 1988), turned out to be problematic for three reasons. First, there is only one potent blocker of aquaporins, mercury, and even mercury is not effective for all aquaporin isoforms (Knepper, 1994). Second, the application of mercury at a concentration reported to be effective (Ishibashi et al., 1997; Preston

et al., 1993) was cytotoxic within the time course of our Ussing experiments on MDCK cells. Third, the inhibitory action of mercury on junctional proteins is unknown.

Direct approaches to determine paracellular water permeability are technically difficult. Apart from analytical calculations (Weinstein and Stephenson, 1981a; Weinstein and Stephenson, 1981b), two experimental approaches have been reported: the fluid-phase fluorescent tracer technique in combination with confocal microscopy (Segawa et al., 2002) and optical methods for visualizing fluid movement in the lateral intercellular space (Kovbasnjuk et al., 1998). These investigations yielded, in part, contrasting results. None of these studies related the results to the molecular composition of the TJ.

In this study, we made no attempts to distinguish technically between the routes for water transport, but applied a selective molecular perturbation of the TJ that resulted in changed ion permeability, and measured overall transepithelial water flux before and after that perturbation. Perturbation was overexpression of either claudin-2 or claudin-10b, as both form cation channels within the TJ of MDCK C7 cells, a tight renal epithelial cell line that lacks endogenous expression of these TJ proteins.

TJs are composed of different transmembrane proteins, including occludin and members of the claudin family. TJ barrier properties vary dramatically (Anderson and Van Itallie, 1995; Schneeberger and Lynch, 1992), depending mainly on the tissue- and segment-specific expression of claudins (Van Itallie et al., 2003). Many claudins support the epithelial barrier function, whereas others form paracellular channels (Van Itallie and Anderson, 2006). The expression of claudin-2 is typical of leaky epithelia with constantly

high water-transport rates, such as proximal tubules and the small intestine (Enck et al., 2001; Rahner et al., 2001; Van Itallie et al., 2003). We have previously demonstrated that claudin-2 forms a cation-selective channel and thus determines the paracellular cation permeability of epithelia (Amasheh et al., 2002). Hence, claudin-2 was our first candidate for analyzing a possible involvement in paracellular water flux. Claudin-10b also mediates significant permeability to small monovalent cations (Günzel et al., 2009; Van Itallie et al., 2006). It is expressed in many epithelial tissues, including those segments of the loop of Henle that are impermeable to water.

In our study, we attempt to answer the question whether TJs are involved in transepithelial water flux and, if so, whether or not the paracellular flux of water and cations are coupled.

Results

Analysis of claudin-2- and claudin-10b-transfected cells

Stably transfected MDCK C7 cells were tested for protein expression using western blot analysis (Fig. 1). The C7-CLDN2 and C7-Cldn10b cells showed pronounced expression of these TJ proteins, whereas no endogenous expression of claudin-2 and claudin-10b could be detected in the respective vector controls. Subcellular localization of the transfected claudins was analyzed by immunofluorescence studies in combination with confocal microscopy (Fig. 2). Double staining of claudin-2 or claudin-10b

with the TJ-marker occludin revealed colocalization of these proteins, seen in the merged views and Z-scans. This indicates the localization of the transfected claudins within the TJ.

Further western blots of the transfected cells show the expression of endogenous claudins known to be expressed in MDCK C7 cells, as well as the expression of AQP water channels. As shown in Fig. 1A, the expression levels of claudin-1, -3, -4, -5, -7 and -8 were unchanged in C7-CLDN2 and C7-Cldn10b cells in comparison to mock-transfected cells. In addition, no changes in the expression of AQP-1, AQP-3 and AQP-4 could be observed (Fig. 1B). Thus, transfection with claudin-2 or claudin-10b affected neither the composition of endogenous claudins within the TJ, which determines barrier function and might influence paracellular water flux, nor AQP expression and therewith transcellular water transport.

Effect of exogenous claudin expression on transepithelial resistance and cation permeability of MDCK C7 cells

Using chamber experiments were carried out to analyze R^t (transepithelial resistance; TER) and ion permeabilities (Fig. 3). R^t was strongly reduced in MDCK C7 cell layers transfected with human claudin-2 or mouse claudin-10b (Fig. 3A). For analysis of claudin-2-transfected cells, we employed two clones with different claudin-2 expression. Clone 6 exhibited strong claudin-2 signals and markedly reduced R^t values of $262 \pm 12 \Omega \cdot \text{cm}^2$ ($n=6$), compared to $1996 \pm 302 \Omega \cdot \text{cm}^2$ ($n=5$) for vector controls, whereas clone 12 showed an R^t of $1148 \pm 33 \Omega \cdot \text{cm}^2$ ($n=14$), due to relatively lower claudin-2 expression (see below). A similar reduction in R^t was observed in claudin-10b-transfected cells (C7-Cldn10b, $404 \pm 72 \Omega \cdot \text{cm}^2$, $n=6$; C7-vector 2, $1735 \pm 274 \Omega \cdot \text{cm}^2$, $n=5$).

For both transfectants and vector controls, multiple clones were generated. All clones showed similar results for each group. For the sake of clarity, only one clone from each group was presented in all figures: clone 6 representing C7-CLDN2 cells and clone 1 representing C7-Cldn10b cells. Clones 11, 12 (C7-CLDN2) and 2 (C7-Cldn10b) served as additional clones. Only additional clone 12, which exhibited lower claudin-2 expression, showed variation,

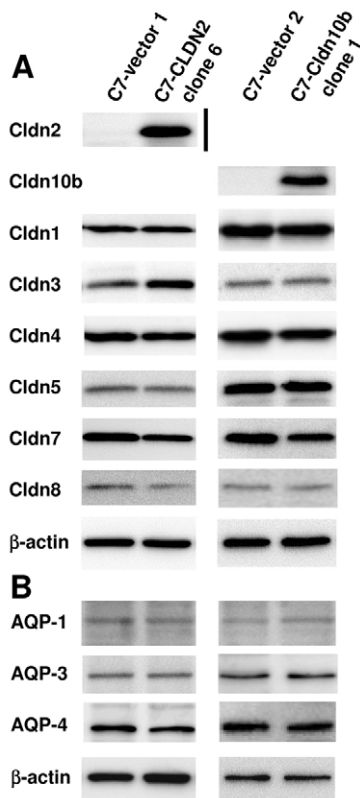


Fig. 1. Claudin and AQP expression in MDCK cells. (A) Western blot analysis of the expression of claudin-2, claudin-10b and endogenous claudins in vector controls and C7-CLDN2 and C7-Cldn10b cells. (B) Western blot analysis of AQP-1, AQP-3 and AQP-4 expression in vector controls and C7-CLDN2 and C7-Cldn10b cells. Equal loading of each lane was verified by β -actin staining.

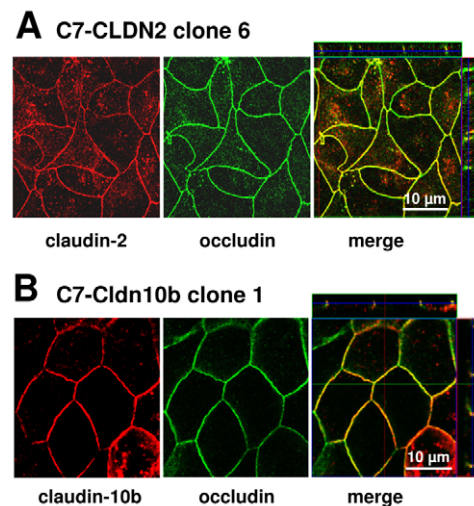


Fig. 2. Analyses of the subcellular distribution of transfected claudins. Immunofluorescence staining of (A) claudin-2 (red) or (B) claudin-10 (red) together with occludin (green) in transfected MDCK C7 cells demonstrates colocalization (yellow) of the claudins with the TJ-marker occludin. Z-scans confirm the localization of the claudins within the TJ.

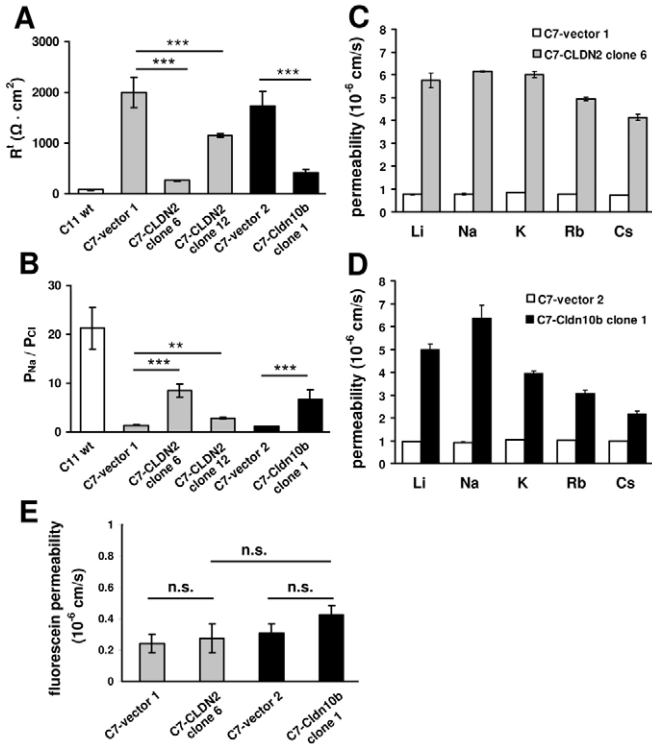


Fig. 3. Transepithelial resistance, and ion and fluorescein permeabilities of wild-type, transfected and mock-transfected MDCK cells. (A) Ussing chamber experiments were performed to analyze transepithelial resistance in wild-type, transfected and mock-transfected MDCK C7 cells and, for comparison, in MDCK C11 cells with endogenous claudin-2 expression ($n=5-14$). (B) Ratio of Na^+ and Cl^- permeability, $P_{\text{Na}}/P_{\text{Cl}}$ ($n=6-27$). (C,D) Changes in the permeability of alkali-metal ions in C7-CLDN2 (C) and C7-Cldn10b (D) cells. Permeabilities were derived from the measurement of dilution and bi-ionic potentials ($n=4-27$), and calculated by means of the Goldman-Hodgkin-Katz equation. (E) Fluorescein permeability of C7-vector controls and C7 cells transfected with claudin-2 or claudin-10b was calculated from fluorescein fluxes.

as its permeability effects were accordingly lower (compare Fig. 3A,B; supplementary material Fig. S1A) (and see below).

For comparison, we analysed cells with very high endogenous expression of claudin-2, MDCK C11, and, as expected, found R^t to be even lower ($78 \pm 7 \Omega \cdot \text{cm}^2$, $n=10$) than in C7-CLDN2 clone 6.

The decrease in R^t was associated with a strong increase in permeability to small monovalent cations, but not to anions (Fig. 3C,D). The ratio of Na^+ and Cl^- permeability ($P_{\text{Na}}/P_{\text{Cl}}$) was approximately 1 in vector controls, indicating no charge selectivity. By contrast, $P_{\text{Na}}/P_{\text{Cl}}$ values in C7-CLDN2 cells were 8.5 ± 1.3 for clone 6 ($n=7$) and 2.8 ± 0.2 for clone 12 ($n=6$) and, in C7-Cldn10b cells, 6.7 ± 2.0 ($n=12$), indicating strong selectivity for cations over anions. This was more pronounced in C7-CLDN2 clone 6 than in clone 12 with the stronger claudin-2 expression (Fig. 3B). There were no differences in R^t values and Na^+ permeabilities between C7-CLDN2 clone 6 and C7-Cldn10b cells.

The permeability sequence for monovalent cations was equivalent to Eisenman sequence IX ($\text{Na}^+ > \text{K}^+ > \text{Li}^+ > \text{Rb}^+ > \text{Cs}^+$) in C7-CLDN2 cells and to Eisenman sequence X ($\text{Na}^+ > \text{Li}^+ > \text{K}^+ > \text{Rb}^+ > \text{Cs}^+$) in C7-Cldn10b cells (Eisenman and Horn, 1983). In vector controls, no clear ranking of permeabilities for alkali metal ions could be observed.

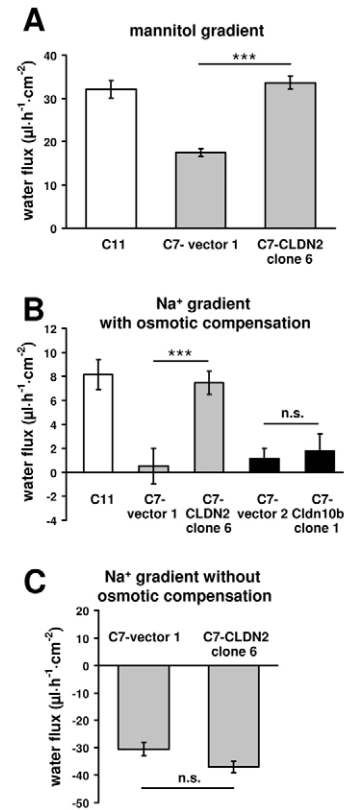


Fig. 4. Water flux in MDCK cells stimulated by an osmotic or ionic gradient. (A) Water flux induced by a gradient of 100 mM mannitol on the apical side of the cell layer ($n=7-13$) was dramatically increased in claudin-2-expressing MDCK cells (C11 and C7-CLDN2). (B) Water flux induced by a NaCl gradient (high basolateral NaCl concentration, $n=7-9$). The osmotic difference was compensated by the addition of 160 mM mannitol to the apical side. Again, water flux was greatly increased in claudin-2-expressing cells, whereas no effect could be observed in claudin-10b-expressing cells. (C) Water flux induced by a NaCl gradient (high basolateral NaCl concentration) without osmotic compensation ($n=8-10$). Under these conditions, water flux was directed from the apical to the basolateral compartment (negative values), following the osmotic gradient. Water flux was not increased in claudin-2-expressing cells; the observed flux is assumed to predominantly reflect the transcellular flux component.

In contrast to the increased cation permeability of cells transfected with claudin-2 or claudin-10b, no differences in permeability to the paracellular marker fluorescein (332 Da) could be observed between C7-vector controls and C7-CLDN2 and C7-Cldn10b cells (Fig. 3E).

Water flux in MDCK cells induced by an osmotic or ionic gradient

Water flux was analyzed in a specially designed Ussing chamber. For the induction of water flux by an osmotic gradient, 100 mM mannitol was added to the apical solution (Table 1). Under these conditions, water flux was much higher in C7-CLDN2 cells than in vector controls and comparable to that in MDCK C11 cells with high endogenous claudin-2 expression (Fig. 4A). Calculated water permeability was $1.6 \pm 0.3 \times 10^{-3} \text{ cm/s}$ and $4.9 \pm 0.3 \times 10^{-3} \text{ cm/s}$ for MDCK C7 and MDCK C11, respectively, and $5.2 \pm 0.2 \times 10^{-3} \text{ cm/s}$

Table 1. NaCl and mannitol concentration (in millimolar units) in water-flux measurements

	NaCl (apical)	NaCl (basolateral)	Mannitol (apical)	Mannitol (basolateral)
Osmotic gradient	145	145	100	0
Ionic gradient, with osmotic compensation	65	145	160	0
Ionic gradient, without osmotic compensation	65	145	0	0
Osmotic and ionic gradient	65	145	260	0

for C7-CLDN2. Thus, osmotically induced water permeability is enhanced by claudin-2.

Water flux induced by mannitol was independent of the direction of the osmotic gradient, as shown in MDCK C11 and MDCK C7 cells. When mannitol was added to the basolateral side of the cells, water flowed in the opposite direction, but the absolute fluxes were not different (MDCK C11: $32.1 \pm 2.0 \mu\text{l}\cdot\text{hour}^{-1}\cdot\text{cm}^{-2}$, $n=7$ versus $-33.3 \pm 3.0 \mu\text{l}\cdot\text{hour}^{-1}\cdot\text{cm}^{-2}$, $n=3$; MDCK C7: $10.6 \pm 1.7 \mu\text{l}\cdot\text{hour}^{-1}\cdot\text{cm}^{-2}$, $n=6$ versus $-11 \pm 2.6 \mu\text{l}\cdot\text{hour}^{-1}\cdot\text{cm}^{-2}$, $n=3$).

In further experiments, water transport was induced by a gradient (80 mM) of NaCl, with the high NaCl concentration (145 mM) in the basolateral compartment and osmotic compensation by 160 mM mannitol on the apical side (Table 1). In MDCK cells, no transcellular Na^+ transport occurs in the basolateral to apical direction. With the basolateral to apical Na^+ gradient, the effect of

paracellular Na^+ movement on water flux was isolated. Under these conditions, water flux was analyzed in C7-CLDN2 and C7-Cldn10b cells to test whether water permeability is dependent on the Na^+ permeability of the TJ. No water flux was observed in C7-vector cells, whereas the claudin-2-expressing cells, C7-CLDN2 and MDCK C11, showed a small amount of water transport in the absence of any osmotic gradient (Fig. 4B). By contrast, no increase in water flux could be observed in cells transfected with claudin-10b, although Na^+ permeability was similar to that of C7-CLDN2 cells. Thus, the Na^+ permeability of TJs was not simply linked to water permeability – paracellular water permeability required claudin-2 within the TJ.

When the low NaCl concentration (65 mM) in the apical compartment was not osmotically compensated by mannitol (Table 1), the Na^+ gradient and the osmotic gradient opposed each other. Under these conditions, water flux in the apical to basolateral direction induced by the resulting osmotic gradient of 160 mOsm/l showed no difference between C7-vector 1 and C7-CLDN2 cells (Fig. 4C). This is assumed to be due to a compensatory effect of these opposing gradients on paracellular water flux. The residual water flux observed under these conditions most likely reflects the transcellular flux driven by the osmotic gradient.

Water transport in MDCK cells induced by the combination of osmotic and ionic gradients

If the above assumption was correct, the combination of osmotic gradient (with mannitol) and NaCl gradient (Table 1) should exert an additive effect on water flux. This was experimentally verified (Fig. 5A). Under these test conditions, the water flux of the two C7-CLDN2 clones was compared. Water flux in both clones was higher than in vector controls, but there was a large difference between the clones that corresponded to differences in claudin-2 expression (Fig. 5B,C). Both water flux and claudin-2 expression were more pronounced in C7-CLDN2 clone 6. Thus, water flux in CLDN2-transfected cells strongly depends on the amount of claudin-2 within the TJ.

Water flux under these conditions was also examined in C7-Cldn10b cells. No differences between vector controls and claudin-10b-transfected cells could be observed. These data confirm the results obtained in the presence of a NaCl gradient. Thus, water flux through claudin-10b could not be induced by either an ionic or an osmotic gradient.

Under these experimental conditions, water flux in a second clone of each vector control and C7-Cldn10b cells was investigated. There was no significant difference between the clones (supplementary material Fig. S1).

The use of lactulose instead of mannitol did not change water flux under these conditions (supplementary material Fig. S2).

Na^+ flux induced by an osmotic gradient in C7-CLDN2 and C7-Cldn10b cells

To examine whether water flux driven by an osmotic gradient could induce paracellular Na^+ movement, flux measurements with

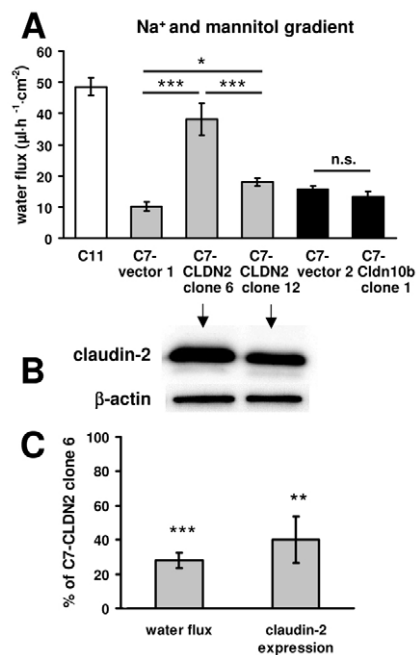


Fig. 5. Water flux in MDCK cells stimulated by a combined osmotic and ionic gradient. (A) Water flux induced by a gradient of 100 mM mannitol (apical) and a NaCl gradient (high basolateral NaCl). Under these conditions, water transport in two C7-CLDN2 clones (clone 6 and clone 12) was increased compared with that in the corresponding control (vector 1). The magnitude of the increase correlated with the amount of claudin-2 detected by western blotting. Claudin-10b-expressing cells showed no increase in water flux ($n=7-11$). (B) Western blot analysis of claudin-2 expression in C7-CLDN2 clones 6 and 12. Equal loading of each lane was verified by β -actin staining. (C) Direct comparison of claudin-2 expression, quantified with densitometric analysis of western blots, and water flux in C7-CLDN2 clones 6 and 12 (C7-CLDN2 clone 6=100%, $n=5$). To determine claudin-2-mediated water flux, the baseline flux measured in C7-vector 1 was subtracted from the water flux in the two claudin-2 clones prior to calculating the ratio.

^{22}Na were performed. ^{22}Na flux in the basolateral to apical direction was measured before and after application of 100 mM mannitol to the apical compartment of the cells. As expected, Na^+ flux under steady-state conditions was much higher in cells expressing the cation channels claudin-2 and claudin-10b than in vector controls (data not shown). The osmotic water flux triggered by mannitol had no effect on the Na^+ flux in vector controls and C7-Cldn10b cells, whereas an increase in flux could be observed in C7-CLDN2 cells (Fig. 6). Thus, only in claudin-2-expressing cells did paracellular water flux occur after application of mannitol, inducing Na^+ movement through the TJ by a solvent-drag mechanism.

Morphometric analysis of TJ ultrastructure in transfected MDCK C7 cells

Morphometric analysis of TJs examined by freeze-fracture electron microscopy revealed no ultrastructural changes after introduction of claudin-2 or claudin-10b within the TJ (Table 2). The meshwork pattern of TJ strands in C7-CLDN2 and C7-Cldn10b cells was similar to that in vector controls (Fig. 7). Furthermore, no difference in the relative occurrence and number of strands between vector controls and claudin-2- or claudin-10b-transfected cells was found (Fig. 8). The same was seen for the number of breaks per strand. The number of particle-type strands varied between 0 and 1 in all groups, indicating a prevalence of continuous strands. Thus, the increased water flux in C7-CLDN2 cells, compared to control cells and claudin-10b-transfected cells, was not caused by changes in gross TJ morphology.

Discussion

This present study clearly proves that TJs are able to participate in transepithelial water flux. Moreover, the analysis of transepithelial

water flux after perturbation of the TJ with claudin-2 or claudin-10b revealed that the water permeability of TJs strongly depends on the claudin composition of the TJ. Claudin-2, but not claudin-10b, confers water permeability on the epithelial cell layer, although both claudins form paracellular cation channels.

Functional changes after transfection with claudin-2 and claudin-10b

Transfection of MDCK C7 cells with human claudin-2 or mouse claudin-10b resulted in correct assembly of these proteins within the TJ, indicated by colocalization with the TJ-marker occludin. In accordance with previous experiments on mouse and dog claudin-2 (Amasheh et al., 2002; Furuse et al., 2001), and human and mouse claudin-10b (Günzel et al., 2009; Van Itallie et al., 2006), we found a marked decrease in transepithelial resistance and an increase in permeability to monovalent cations in the transfected cells. In contrast to the enhanced cation permeability, no changes in the permeability of the paracellular marker fluorescein could be observed. Western blot analysis revealed that the transfection with exogenous claudins did not affect the expression of endogenous claudins in these cells, so that the changes in cation permeability and transepithelial resistance could be exclusively attributed to the effect of claudin-2 or claudin-10b within the TJ. Changes in TJ ultrastructure, such as strand number, meshwork depth, occurrence of breaks and incidence of particle-type strands, might have affected TJ barrier function. In the present study, we found no significant differences in TJ ultrastructure between vector controls and cells transfected with claudin-2 or claudin-10b with regard to any of the morphometric parameters. These results are in accordance with the unchanged fluorescein permeability. Thus, we conclude that functional changes in the transfected cells are not due to obvious morphological changes of the TJ, but rather to an intrinsic function of claudin-2 or claudin-10b within the intact TJ.

Transepithelial water transport

Large volumes of water are absorbed across gastrointestinal and renal epithelia. Water flux is coupled to transepithelial solute absorption. Solute-coupled water transport is also important in many epithelia. Several mechanisms have been suggested for the coupling between water and solute transport that affect either the transcellular pathway [osmotic coupling in intraepithelial compartments (Curran, 1960; Curran and Macintosh, 1962; Diamond and Bossert, 1967) and coupling by specific transport proteins, such as the Na^+ -glucose transporter SGLT1 (Loo et al., 1996; Zeuthen et al., 1997)] or the paracellular pathway [electro-osmotic coupling within the TJ (Fischbarg et al., 2006) and junctional fluid transfer across the TJ (Hill and Shachar-Hill, 2006)].

Transcellular water flux is mediated by transmembrane AQP water channels. In humans, 11 AQPs (AQP-0 to AQP-10) have

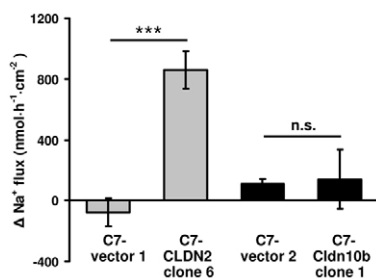


Fig. 6. Na^+ flux in transfected MDCK C7 cells. ^{22}Na flux in the basolateral to apical direction was measured in vector controls, and C7-CLDN2 and C7-Cldn10b cells before and after application of 100 mM mannitol to the apical compartment of the Ussing chamber ($n=3-8$). An increase in Na^+ flux after mannitol application could be observed in C7-CLDN2 cells, but not in C7-Cldn10b cells and vector controls.

Table 2. Morphometric analysis of TJ ultrastructure

	C7-vector 1 ($n=11$)	C7-CLDN2 clone 6 ($n=24$)	C7-vector 2 ($n=16$)	C7-Cldn10b clone 1 ($n=21$)
Number of horizontal strands	2.93±0.18	3.03±0.20	3.13±0.24	3.15±0.21
Vertical meshwork depth (nm)	125.3±18.9	147.1±17.0	120.7±11.9	156.2±20.3
Breaks per μm strand length	0.23±0.16	0.23±0.11	0.32±0.17	0.24±0.12
Particle-type/continuous strands	0/11	1/23	1/15	0/21

There were no significant differences between the groups for any of the analyzed parameters.

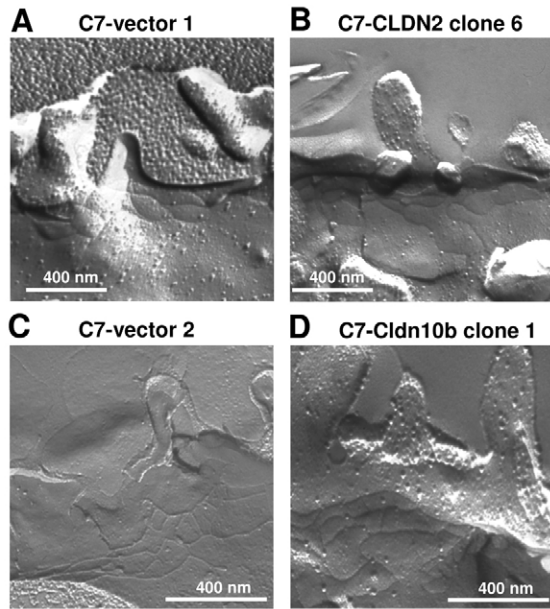


Fig. 7. Freeze-fracture electron microscopy of TJ strands. Freeze-fracture electron microscopy images demonstrate that transfection with claudin-2 (B) or claudin-10b (D) cells did not change the TJ ultrastructure in comparison with vector controls (A,C). All replicas showed a regular meshwork with almost continuous strands and nearly no strand breaks.

been identified and functionally characterized (King et al., 2004; Kozono et al., 2002). In the kidney, AQP-1, -2, -3, -4, -6, -7 and -8 are expressed with different segmental localization (Elkjaer et al., 2001; Kwon et al., 2001). AQP-1 is expressed in the apical and basolateral membranes, whereas AQP-3 and -4 are only present in the basolateral membrane (Deen and van Os, 1998). Studies on AQP-1-knockout mice indicate the existence of a paracellular pathway for osmotically driven transepithelial water transport (Schnermann et al., 1998).

Despite these results, paracellular water transport across the TJ is discussed controversially. Since the discovery of the considerable ion permeability of the TJ, many indirect methods have been applied in various studies to determine water flux across the TJ barrier (Spring, 1998). Evidence against paracellular flux appeared in a study that used a complex optical-computational technique to directly visualize the flow velocity within the lateral intercellular spaces of MDCK cells and thus

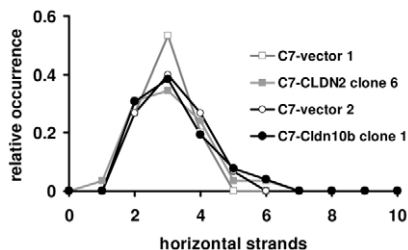


Fig. 8. Relative occurrence of horizontal strands. Morphometric analysis of TJ ultrastructure revealed that transfection with claudin-2 or claudin-10b did not alter the relative occurrence of horizontal strands.

determine fluid movement across the TJ (Kovbasnjuk et al., 1998). This study failed to detect paracellular water flux in MDCK cells. However, the osmotic gradient used to induce fluid flux was low, so that fluid movements might have been too small to be observed.

Other studies obtained evidence for the existence of paracellular water flux in leaky epithelia (Fischbarg et al., 2006; Shachar-Hill and Hill, 2002). Fischbarg et al. (Fischbarg et al., 2006) demonstrated in leaky corneal endothelium that fluid is transported by means of the paracellular route by a mechanism requiring junctional integrity, which was attributed to electro-osmotic coupling at the junctions. Fluid movement could be produced by electrical current and the direction of movement could be reversed by current reversal or by changing the TJ electrical charges using poly-L-lysine (Ma et al., 2007).

Our data clearly demonstrate the qualitative existence of claudin-2-mediated water permeability. However, the question arises about the quantitative significance of these effects in epithelia. A comparison of kidney tubule epithelia with MDCK cells reveals considerably higher water permeabilities for kidney tubules. In cortical collecting tubules, transepithelial water permeability in the absence of vasopressin ranged from 1.2×10^{-3} cm/s (Kuwahara et al., 1991) to 7.0×10^{-3} cm/s (Sands et al., 1987). In proximal tubules with strong expression of claudin-2 (Kiuchi-Saishin et al., 2002), water permeability is much higher; the values varied from 35×10^{-3} cm/s (Quigley and Baum, 1996) to 150×10^{-3} cm/s (Schnermann et al., 1998).

In the present study, a value of 1.6×10^{-3} cm/s was obtained for MDCK C7 cells, a cell-culture model for tight epithelia. Water permeability of MDCK C11 cells with endogenous claudin-2, a model for leaky epithelia, was considerably higher (4.9×10^{-3} cm/s). Similarly high values were obtained for MDCK C7 cells transfected with claudin-2, so the increased water permeability of MDCK C11 is consistent with paracellular water permeability mediated by claudin-2.

The water permeability of the MDCK cell-culture model cannot be directly compared with that of kidney tubules, as indicated by the several-fold higher R^f of MDCK cells compared with kidney tubule epithelium. In leaky epithelia, the transepithelial resistance is mainly determined by the properties of the paracellular pathway. For kidney proximal tubules, R^f values of between 4.5 (Melis et al., 1993) and $16 \Omega \cdot \text{cm}^2$ (Bello-Reuss, 1986) have been reported, whereas in the present study average R^f values for MDCK C11 cells and claudin-2-transfected MDCK C7 cells were $78 \Omega \cdot \text{cm}^2$ and $262 \Omega \cdot \text{cm}^2$, respectively. Because in leaky epithelia, the R^f is mainly determined by the properties of the paracellular pathway, the differences in R^f values between cultured cells and native tissue might reflect the different water permeabilities.

Water transport after perturbation of the tight junction

In claudin-2-transfected cells, but not in claudin-10b-transfected cells, water flux could be induced by a Na^+ gradient in the absence of any osmotic gradient. Thus, in the presence of claudin-2, paracellular Na^+ flux induced water flux through the TJ. Conversely, the osmotic-gradient-induced water flux causes Na^+ movement through the TJ. These results indicate the coupling of Na^+ and water flux, which suggests that Na^+ and water permeate the paracellular barrier the same way, namely through the claudin-2 channel. The coupling ratio in the presence of 100 mM mannitol, calculated from the difference in water flux between C7-vector 1 and C7-CLDN2 and the mannitol-induced increase in Na^+ flux in

C7-CLDN2, is approximately 1 Na⁺ : 1000 H₂O, indicating a ratio far exceeding that of hydrated Na⁺, which is 1:6 only.

By contrast, this coupling mechanism does not exist for claudin-10b. In C7-Cldn10b cells, no changes in water flux could be observed, although the Na⁺ permeability of C7-Cldn10b and C7-CLDN2 cells is very similar. Thus, the claudin-10b-based paracellular cation channel is not permeable to water. These functional properties of both claudins are in keeping with their expression in the kidney: claudin-2 in proximal tubules with high water and Na⁺ absorption; and claudin-10b in water-impermeable parts of the loop of Henle with high Na⁺ absorption, among other segments.

The observed effects, that is, high Na⁺ permeability in the presence of claudin-10b, and high Na⁺ and high water permeability in the presence of claudin-2, are exclusively due to the presence of these claudins within the TJ. All other parameters contributing to water permeability and barrier properties, for example, expression of AQP and endogenous claudins and TJ morphology, were unchanged in the transfected cells.

Claudin-based cation channels

Recent investigations revealed that epithelial TJs contain charge- and size-selective pores, which control the paracellular flux of charged and uncharged solutes. The paracellular flux occurs through two distinct pathways: one high-capacity pathway with size-restrictive pores and one low-capacity pathway that is size independent, at least for substances with radii of up to 7 Å (Van Itallie et al., 2008; Watson et al., 2001). The physical basis of the low-capacity pathway is not yet completely understood, whereas the high-capacity pathway is well described. It consists of small pores with radii of ~4 Å, and is responsible for the flux of small charged and uncharged solutes. Expression of claudin-2 affects only the high-capacity pathway, by inducing an increase in pore number and a change in charge selectivity (Van Itallie et al., 2008). In a recent attempt to model the claudin-2-induced channel (Yu et al., 2009), the pore diameter, calculated from permeability to organic cations and from the relative permeabilities of alkali-metal ions, was about 6.5 Å. This feature would allow uncharged water molecules, with a molecular diameter of about 2.8 Å, to permeate through the pore. Because the pore diameter is smaller than the diameter of hydrated alkali-metal ions (Nightingale, 1959), monovalent ions have to shed part of their hydration shell to penetrate the claudin-2 pore, as mirrored in Eisenman sequence IX found for claudin-2 (Eisenman and Horn, 1983). Unhydrated alkali-metal ions with a crystal diameter between 1.2 and 3.4 Å (Nightingale, 1959) can easily pass through the pore, which might explain the small differences in permeability between these ions. The energy of dehydration must be compensated by an energetically favorable interaction with a charged site within the pore. For claudin-2, amino acid D65 in the first extracellular loop has been reported to form this interaction site (Angelow and Yu, 2009; Yu et al., 2009).

No similar modeling has yet been carried out for the cation channel formed by claudin-10b. However, the alkali-metal Eisenman sequence X found for claudin-10b indicates the permeation of partially dehydrated or unhydrated ions. The Na⁺ permeability of claudin-2- and claudin-10b-based pores is very similar, but their permeability to the ion with the largest crystal diameter, Cs⁺, was much lower in C7-Cldn10b cells. This might be due to a smaller pore diameter and/or a different charge distribution within the first extracellular loop of this claudin. As

stated by Eisenman and Horn (Eisenman and Horn, 1983), the absolute selectivity among cations depends upon the distance between anionic binding sites and is stronger for closely spaced than for widely separated sites. With five negative charges within the first extracellular loop of claudin-10b (59 amino acids), the density of negative charges is higher than for claudin-2 (3 of 53 amino acids have negative charge), which might be a deciding factor for the stronger selectivity among the group of monovalent cations found for claudin-10b. It remains to be elucidated in future studies whether or not these parameters affecting charge selectivity and ion permeability are important for water permeability.

To date, nothing is known about the molecular structure of the claudin-based channels. Recent investigations have demonstrated homo- and hetero-typic interactions of claudins (Blasig et al., 2006; Daugherty et al., 2007; Furuse et al., 1999; Piontek et al., 2008), suggesting that the paracellular channels are formed by claudin oligomers. Thus, the cation channels in the transfected cells could be composed of solely the exogenous claudins (homotypic interaction) or a combination of exogenous claudins and endogenous claudins (heterotypic interaction, because the transfected claudins are not endogenously expressed in the cells). Two models of homotypic interaction of claudin-2 or heterotypic interaction with claudin-1 or claudin-4, which constitutes aqueous pores, are proposed by Furuse et al. (Furuse et al., 2001). The exact nature of interaction that is essential for cation and water permeability has not yet been clarified.

Conclusions

In summary, the presence of the paracellular cation channel claudin-2, but not the paracellular cation channel claudin-10b, within the TJ of a tight epithelium caused enhanced transepithelial water flux, which occurs through the TJs and is coupled to paracellular Na⁺ flow. Thus, this study clearly proves that TJs are water permeable and that the paracellular water permeability is determined by the molecular composition of the TJ. We conclude that the cation channel claudin-2 forms a paracellular water channel that mediates water transport across the TJs in leaky epithelia.

Materials and Methods

Cell cultures

Two subclones of Madin-Darby canine kidney (MDCK) cells, high-resistance MDCK C7 and low-resistance MDCK C11 (Gekle et al., 1994), were grown in 25 cm² culture flasks containing MEM-EARLE (PAA Laboratories, Pasching, Austria) supplemented with 10% (v/v) FBS, 100 mg/ml streptomycin and 100 U/ml penicillin (Biochrom, Berlin, Germany). Cells were cultured at 37°C in a humidified 5% CO₂ atmosphere. For water flux measurements and western blot analysis, cell monolayers were cultured on porous culture-plate inserts (Millicell-HA, pore size 0.45 µm, effective area 0.6 cm²; Millipore, Schwalbach, Germany) for 5 to 7 days before they were used for experiments. Experiments were performed on monolayers of wild-type MDCK C11 and MDCK C7 cells, and stably transfected MDCK C7 cells. The culture medium for transfected cells was supplemented with 600 µg/ml G418 (PAA Laboratories).

Cloning of claudin-2 and claudin-10b, generation of expression constructs and transfection

For generation of claudin-2 expression constructs, total RNA was obtained from T84 cells (human colon carcinoma cell line; ATCC, Manassas, VA) using RNazol B reagent (WAK-Chemie, Steinbach, Germany) according to the manufacturer's protocols. First-strand cDNA was obtained by reverse transcriptase reaction (M-MLV; Gibco BRL, Bethesda, MD) employing oligo-(dT) primers. Subsequent PCR using primers derived from the human claudin-2 sequence (5'-ATGGCCTCTC-TTGGCCTCAA-3'; 3'-TCACACATACCCTGTGAGGCT-5') resulted in a product encompassing the complete claudin-2 cDNA. The PCR product was cloned into the pCR 2.1-TOPO vector (Invitrogen), verified by sequencing and subsequently subcloned into the eukaryotic expression vector pFLAG-CMV4 (Sigma). The generation of claudin-10b expression constructs has recently been described in detail

(Günzel et al., 2009). The resulting constructs were subcloned into the mammalian expression vector pcDNA3.1(+). (Invitrogen).

MDCK C7 cells were stably transfected with human claudin-2 (C7-CLDN2) and mouse claudin-10b (C7-Cldn10b) using Lipofectamine plus or Lipofectamine 2000 (Invitrogen), respectively. G418-resistant cell clones were screened for exogenous claudin expression by western blot analysis and immunofluorescence studies (see below). MDCK C7 cells transfected with the empty vector served as controls [C7-vector 1 with pFLAG-CMV-4; C7-vector 2 with pcDNA3.1(+)].

Western blot analysis

Western blot analysis was performed as recently reported (Amasheh et al., 2002). Cells grown on culture-plate inserts were scraped and homogenized in lysis buffer containing 20 mM TRIS, 5 mM MgCl₂, 1 mM EDTA, 0.3 mM EGTA and 1× complete protease inhibitor mixture (Roche), and passed through a 26 gauge 1/2 needle. The membrane fraction was obtained by centrifugation for 5 minutes at 500 g (4°C) and subsequent centrifugation of the resulting supernatant for 30 minutes at 43,000 g (4°C). Pellets were resuspended in lysis buffer, and the protein concentration was determined by the BCA (bicinchoninic acid) method [reagents were purchased from Pierce (Perbio Science, Bonn, Germany)] and quantified with a plate reader (Tecan Deutschland, Crailsheim, Germany). Aliquots of 10 µg protein samples were separated by 12.5% SDS-polyacrylamide gel electrophoresis and blotted onto a polyvinylidene fluoride membrane for detection of claudins and AQP. After blocking for 2 hours in 5% BSA, membranes were incubated overnight with primary antibodies specific for claudin-1, -2, -3, -4, -5, -7 and -8 (Invitrogen), and AQP-1, -3 and -4 (Santa Cruz, Heidelberg, Germany). Chemiluminescence was induced with a Lumi-LightPLUS western blotting kit (Roche), detected with an LAS-1000 imaging system (Fuji, Tokyo, Japan), and densitometric analysis was performed with quantification software (AIDA, Raytest, Straubenhardt, Germany). Equal protein loading in each lane was verified by staining with β-actin (Sigma-Aldrich). Western blot experiments were performed at least three times on individual cell cultures, with one representative experiment shown.

Immunofluorescence analysis

Immunofluorescence studies were performed with cells grown on coverslips (diameter 13 mm, C7-CLDN2) or on culture-plate inserts (C7-Cldn10b). Confluent monolayers were rinsed with PBS, fixed with methanol at -20°C for 10 minutes and permeabilized with PBS containing 0.5% (v/v) Triton X-100 for 5 minutes. To block non-specific binding sites, cells were then incubated in PBS containing 0.5% (v/v) goat serum (blocking solution; Biochrom) for 30 minutes. All subsequent washing procedures were performed with this blocking solution. After blocking, cells were incubated with primary polyclonal antibodies against claudin-2 or against claudin-10 (rabbit-anti-Cldn2, rabbit-anti-Cldn10; Invitrogen) and monoclonal occludin antibody (mouse-anti-occludin; Invitrogen) diluted in blocking solution (both used at concentrations of 20 µg/ml) for 1 hour at 37°C. After two washes, cells were incubated with secondary antibodies Alexa-Fluor-488-conjugated goat anti-mouse IgG and Alexa-Fluor-594-conjugated goat anti-rabbit IgG (both used at concentrations of 2 µg/ml; Invitrogen) diluted in blocking solution for 30 minutes at 37°C. After two washes, cells were mounted in ProTaq Mount Fluor (BIOCYC, Luckenwalde, Germany). Fluorescence images were obtained with a confocal laser-scanning microscope (Zeiss LSM 510 META, Jena, Germany) at excitation wavelengths of 543 and 488 nm.

Freeze-fracture electron microscopy

Freeze-fracture analysis was carried out as described before (Zeissig et al., 2007). Cells grown on cell-culture inserts were initially fixed with phosphate-buffered glutaraldehyde (2%), then incubated in 10% (v/v) and later in 30% (v/v) glycerol and finally frozen in liquid-nitrogen-cooled Freon 22. The preparations were fractured at -100°C, and shadowed with platinum and carbon in a vacuum evaporator (Denton DV-502, Denton Vacuum, Cherry Hill, NJ). The replicas floating off the samples were bleached with sodium hypochloride, then mounted on copper grids and analyzed using a Zeiss 902A electron microscope (Carl Zeiss NTS, Oberkochen, Germany) with digital camera iTEM Veleta (Olympus Soft Imaging Solutions, Münster, Germany).

Morphometric analysis was performed using coded prints of freeze-fracture electron micrographs (51,000× magnification) of all TJ regions in which both an apical and a contra-apical strand of the meshwork could be clearly distinguished. The distance between these strands was measured as the meshwork depth. Vertical grids were drawn at 200 nm intervals perpendicular to the most apical TJ strand. The number of horizontal strands within the main TJ meshwork was counted at intersections with grid lines. Strand discontinuities of >20 nm within the compact TJ meshwork were defined as 'breaks' and given per micrometer length of horizontally oriented strands. The linearity of strand formation was denoted as 'particle type' or 'continuous'.

Dilution and bi-ionic potential measurements

Dilution and bi-ionic potential measurements for the determination of ion permeabilities were performed in Ussing chambers modified for cell-culture inserts. Water-jacketed gas lifts were filled with 10 ml circulating fluid on each side. Bathing solution contained (in mM) 119 NaCl, 21 NaHCO₃, 5.4 KCl, 1.2 CaCl₂, 1 MgSO₄,

3 HEPES and 10 D(+)-glucose, and was gassed with 95% O₂ and 5% CO₂ to ensure a pH value of 7.4. The temperature of the bathing solution was kept at 37°C. All experimental data were corrected for the resistance of the empty filter and the bathing solution.

Dilution and bi-ionic potentials were measured with modified bathing solution on the apical or basolateral side of the epithelial monolayer. In the modified bathing solution, NaCl was iso-osmotically replaced either by mannitol for calculating Na⁺ and Cl⁻ permeability, or by KCl, LiCl, RbCl or CsCl. Ion permeabilities were calculated by means of the Goldman-Hodgkin-Katz equation, as described by Günzel et al. (Günzel et al., 2009).

Measurement of fluorescein permeability

The permeability of the paracellular marker fluorescein was calculated from flux measurements, which were performed in Ussing chambers under voltage-clamp conditions. Briefly, after equilibration, fluorescein (fluorescein-sodium salt; Sigma-Aldrich) in a final concentration of 100 µM was added apically (donor side), and samples (300 µl) were collected from the basolateral (receiving) side at *t*=30, 60 and 90 minutes, and immediately replaced by fresh standard bath solution. Samples were analyzed as duplicates, using a 96-well plate (140 µl/well) and a plate reader (Spectramax Gemini, Molecular devices). Fluorescence signals were calibrated using defined dilutions in standard bath solution. Flux was calculated as the increase in tracer quantity (corrected for dilution) per time unit and filter area. Permeabilities were calculated as flux/concentration on the donor side.

Measurement of transepithelial water permeability

To measure water permeability, Ussing chambers were modified. Gas lifts were replaced by a chamber with two separated silanized glass tubes. The fluid-filled chamber was heated to maintain a constant temperature of 37°C and a rotary pump ensured constant circulation (2.8 ml/min, Ussing chamber volume 500 µl) and fast fluid exchange in both chambers to minimize the effects of unstirred layers on water permeability. Measurements of transepithelial resistance (*R*_t, Ω·cm²), short-circuit current (*I*_{SC}, µA·cm⁻²) and transepithelial voltage (mV) were recorded by a standard PC with ADC-DAC cards. Impulses of 10 µA and 1 second duration were applied at 25 second intervals to obtain *R*_t. The resistance of the bathing solution and blank filter support was measured prior to each experiment and subtracted. The stability of transepithelial resistance during the experiment was used as an indicator of cell viability. The transepithelial voltage was clamped to 0 mV to avoid effects on ion and water flux.

Cell filters were mounted in Ussing chambers and water-jacketed glass tubes were filled with HEPES-buffered bathing solution on each side. Because the perfusion solution could not be gassed under these experimental conditions, HEPES-buffered solution with the following composition (in mM) was used: 134.6 NaCl, 2.4 Na₂HPO₄, 0.6 NaH₂PO₄, 5.4 KCl, 1.2 MgCl₂, 1.2 CaCl₂, 10.6 HEPES, 10 D(+)-glucose, adjusted to pH 7.4 with approximately 5 mM NaOH; thus, the total NaCl concentration was 144.8 mM.

A transepithelial osmotic gradient was generated with mannitol (100 mM). For experiments with a Na⁺ gradient (80 mM), the 'low-Na⁺' perfusion solution had the same composition except for NaCl (54.6 mM) and 160 mM mannitol was added to compensate for the osmotic difference. For experiments combining osmotic and Na⁺ gradients, 260 mM mannitol was added to the low-NaCl solution. The fluid level in both tubes was monitored by a visual system, ColorView XS (Olympus Soft Imaging Solutions), at time 0 minutes and every 15 minutes over a period of 2 hours. From the difference between the menisci at the registration times, the water flux was calculated. After calibration, the changes in fluid levels were converted into water flux per square centimeter and hour. Water permeability was calculated from $P=J/\Delta c$, where *P* is the permeability (cm/s), *J* is the flux (mol h⁻¹ cm⁻²) and *c* is the concentration (mol/l).

²²Na⁺ flux measurements

Na⁺ flux measurements were performed in Ussing chambers under short-circuited conditions with 2400 kBq/L ²²Na⁺ (PerkinElmer LAS, Rodgau, Germany). After a brief period of equilibration, ²²Na⁺ was added to the perfusion solution in the basolateral reservoir (*t*=0 minutes). Samples (1 ml) were taken from the apical side at 0 minutes (background counts) and then every 30 minutes, and replaced with fresh perfusion solution. After three flux periods, 100 mM mannitol was added to the apical bathing solution to induce water flux and samples were collected for three further flux periods and replaced with perfusion solution containing 100 mM mannitol. In addition, one 100 µl sample was taken from the basolateral side and diluted with 900 µl perfusion solution. All 1 ml samples were subsequently analyzed with gamma-counter 1480 Wizard TM3 (Wallac, Freiburg, Germany).

Statistical analysis

Data are expressed as means ± s.e.m. Statistical analysis was performed using Student's *t*-test and the Bonferroni-Holm correction for multiple comparisons. Significance levels are denoted n.s.=not significantly different, *=*P*<0.05, **=*P*<0.01, ***=*P*<0.001. The number (*n*) refers to the number of experiments.

We thank Detlef Sorgenfrei, Anja Fromm, Susanna Schön and Marianne Boxberger for their expert technical assistance. This work was supported by grants from the Deutsche Forschungsgemeinschaft (DFG FOR 721) and the Sonnenfeld-Stiftung Berlin.

Supplementary material available online at <http://jcs.biologists.org/cgi/content/full/123/11/1913/DC1>

References

- Agre, P., Preston, G. M., Smith, B. L., Jung, J. S., Raina, S., Moon, C., Guggino, W. B. and Nielsen, S. (1993). Aquaporin CHIP: the archetypal molecular water channel. *Am. J. Physiol.* **265**, 463-476.
- Amasheh, S., Meiri, N., Gitter, A. H., Schöneberg, T., Mankertz, J., Schulzke, J. D. and Fromm, M. (2002). Claudin-2 expression induces cation-selective channels in tight junctions of epithelial cells. *J. Cell Sci.* **115**, 4969-4976.
- Anderson, J. M. and Van Itallie, C. M. (1995). Tight junctions and the molecular basis for regulation of paracellular permeability. *Am. J. Physiol.* **269**, 467-475.
- Angelow, S. and Yu, A. S. (2009). Structure-function studies of claudin extracellular domains by cysteine-scanning mutagenesis. *J. Biol. Chem.* **284**, 29205-29217.
- Bello-Reuss, E. (1986). Cell membranes and paracellular resistances in isolated renal proximal tubules from rabbit and *Ambystoma*. *J. Physiol.* **370**, 25-38.
- Blasig, I. E., Winkler, L., Lassowski, B., Mueller, S. L., Zuleger, N., Krause, E., Krause, G., Gast, K., Kolbe, M. and Piontek, J. (2006). On the self-association potential of transmembrane tight junction proteins. *Cell. Mol. Life Sci.* **63**, 505-514.
- Carpi-Medina, P. and Whittembury, G. (1988). Comparison of transcellular and transepithelial water osmotic permeabilities (Pos) in the isolated proximal straight tubule (PST) of the rabbit kidney. *Pflügers Arch.* **412**, 66-74.
- Curran, P. F. (1960). Na, Cl, and water transport by rat ileum in vitro. *J. Gen. Physiol.* **43**, 1137-1148.
- Curran, P. F. and Macintosh, J. R. (1962). A model system for biological water transport. *Nature* **193**, 347-348.
- Daugherty, B. L., Ward, C., Smith, T., Ritzenthaler, J. D. and Koval, M. (2007). Regulation of heterotypic claudin compatibility. *J. Biol. Chem.* **282**, 30005-30013.
- Deen, P. M. and van Os, C. H. (1998). Epithelial aquaporins. *Curr. Opin. Cell Biol.* **10**, 435-442.
- Diamond, J. M. and Bossert, W. H. (1967). Standing-gradient osmotic flow. A mechanism for coupling of water and solute transport in epithelia. *J. Gen. Physiol.* **50**, 2061-2083.
- Eisenman, G. and Horn, R. (1983). Ionic selectivity revisited: the role of kinetic and equilibrium processes in ion permeation through channels. *J. Membr. Biol.* **76**, 197-225.
- Elkjaer, M. L., Nejsum, L. N., Gresz, V., Kwon, T. H., Jensen, U. B., Frokiaer, J. and Nielsen, S. (2001). Immunolocalization of aquaporin-8 in rat kidney, gastrointestinal tract, testis, and airways. *Am. J. Physiol. Renal Physiol.* **281**, 1047-1057.
- Enck, A. H., Berger, U. V. and Yu, A. S. (2001). Claudin-2 is selectively expressed in proximal nephron in mouse kidney. *Am. J. Physiol. Renal Physiol.* **281**, 966-974.
- Fischbarg, J., Diecke, F. P., Iserovich, P. and Rubashkin, A. (2006). The role of the tight junction in paracellular fluid transport across corneal endothelium. Electro-osmosis as a driving force. *J. Membr. Biol.* **210**, 117-130.
- Furuse, M., Sasaki, H. and Tsukita, S. (1999). Manner of interaction of heterogeneous claudin species within and between tight junction strands. *J. Cell Biol.* **147**, 891-903.
- Furuse, M., Furuse, K., Sasaki, H. and Tsukita, S. (2001). Conversion of zonula occludentes from tight to leaky strand type by introducing claudin-2 into Madin-Darby canine kidney I cells. *J. Cell Biol.* **153**, 263-272.
- Gekle, M., Wünsch, S., Oberleitner, H. and Silbernagl, S. (1994). Characterization of two MDCK-cell subtypes as a model system to study principal cell and intercalated cell properties. *Pflügers Arch.* **428**, 157-162.
- Günzel, D., Stuiver, M., Kausalya, P. J., Haisch, L., Krug, S. M., Rosenthal, R., Meij, I. C., Hunziker, W., Fromm, M. and Müller, D. (2009). Claudin-10 exists in six alternatively spliced isoforms that exhibit distinct localization and function. *J. Cell Sci.* **122**, 1507-1517.
- Hill, A. E. and Shachar-Hill, B. (2006). A new approach to epithelial isotonic fluid transport: an osmosensor feedback model. *J. Membr. Biol.* **210**, 77-90.
- Ishibashi, K., Sasaki, S., Fushimi, K., Yamamoto, T., Kuwahara, M. and Marumo, F. (1997). Immunolocalization and effect of dehydration on AQP3, a basolateral water channel of kidney collecting ducts. *Am. J. Physiol.* **272**, 235-241.
- King, L. S., Kozono, D. and Agre, P. (2004). From structure to disease: the evolving tale of aquaporin biology. *Nat. Rev. Mol. Cell Biol.* **5**, 687-698.
- Kiuchi-Saishin, Y., Gotoh, S., Furuse, M., Takasuga, A., Tano, Y. and Tsukita, S. (2002). Differential expression patterns of claudins, tight junction membrane proteins, in mouse nephron segments. *J. Am. Soc. Nephrol.* **13**, 875-886.
- Knepper, M. A. (1994). The aquaporin family of molecular water channels. *Proc. Natl. Acad. Sci. USA* **91**, 6255-6258.
- Kovbasnjuk, O., Leader, J. P., Weinstein, A. M. and Spring, K. R. (1998). Water does not flow across the tight junctions of MDCK cell epithelium. *Proc. Natl. Acad. Sci. USA* **95**, 6526-6530.
- Kozono, D., Yasui, M., King, L. S. and Agre, P. (2002). Aquaporin water channels: atomic structure molecular dynamics meet clinical medicine. *J. Clin. Invest.* **109**, 1395-1399.
- Kuwahara, M., Shi, L. B., Marumo, F. and Verkman, A. S. (1991). Transcellular water flow modulates water channel exocytosis and endocytosis in kidney collecting tubule. *J. Clin. Invest.* **88**, 423-429.
- Kwon, T. H., Hager, H., Nejsum, L. N., Andersen, M. L., Frokiaer, J. and Nielsen, S. (2001). Physiology and pathophysiology of renal aquaporins. *Semin. Nephrol.* **21**, 231-238.
- Loeschke, K. and Bentzel, C. J. (1994). Osmotic water flow pathways across Necturus gallbladder: role of the tight junction. *Am. J. Physiol.* **266**, 722-730.
- Loo, D. D., Zeuthen, T., Chandy, G. and Wright, E. M. (1996). Cotransport of water by the Na⁺/glucose cotransporter. *Proc. Natl. Acad. Sci. USA* **93**, 13367-13370.
- Ma, L., Kuang, K., Smith, R. W., Rittenband, D., Iserovich, P., Diecke, F. P. and Fischbarg, J. (2007). Modulation of tight junction properties relevant to fluid transport across rabbit corneal endothelium. *Exp. Eye Res.* **84**, 790-798.
- Melis, M. S., Malnic, G. and Aires, M. M. (1993). Effect of medium tonicity on transepithelial H(+)-HCO₃-fluxes in rat proximal tubule. *J. Physiol.* **465**, 9-20.
- Nightingale, E. R. (1959). Phenomenological theory of ion solvation. Effective radii of hydrated ions. *J. Phys. Chem.* **63**, 1381-1387.
- Piontek, J., Winkler, L., Wolburg, H., Müller, S. L., Zuleger, N., Piehl, C., Wiesner, B., Krause, G. and Blasig, I. E. (2008). Formation of tight junction: determinants of homophilic interaction between classic claudins. *FASEB J.* **22**, 146-158.
- Poler, S. M. and Reuss, L. (1987). Protamine alters apical membrane K⁺ and Cl⁻ permeability in gallbladder epithelium. *Am. J. Physiol.* **253**, 662-671.
- Preston, G. M., Jung, J. S., Guggino, W. B. and Agre, P. (1993). The mercury-sensitive residue at cysteine 189 in the CHIP28 water channel. *J. Biol. Chem.* **268**, 17-20.
- Quigley, R. and Baum, M. (1996). Developmental changes in rabbit juxtamedullary proximal convoluted tubule water permeability. *Am. J. Physiol.* **271**, 871-876.
- Quigley, R. and Baum, M. (2002). Water transport in neonatal and adult rabbit proximal tubules. *Am. J. Physiol. Renal Physiol.* **283**, 280-285.
- Rahner, C., Mitic, L. L. and Anderson, J. M. (2001). Heterogeneity in expression and subcellular localization of claudins 2, 3, 4, and 5 in the rat liver, pancreas, and gut. *Gastroenterology* **120**, 411-422.
- Sands, J. M., Nonoguchi, H. and Knepper, M. A. (1987). Vasopressin effects on urea and H₂O transport in inner medullary collecting duct subsegments. *Am. J. Physiol.* **253**, 823-832.
- Schneeberger, E. E. and Lynch, R. D. (1992). Structure, function, and regulation of cellular tight junctions. *Am. J. Physiol.* **262**, 647-661.
- Schnermann, J., Chou, C. L., Ma, T., Traynor, T., Knepper, M. A. and Verkman, A. S. (1998). Defective proximal tubular fluid reabsorption in transgenic aquaporin-1 null mice. *Proc. Natl. Acad. Sci. USA* **95**, 9660-9664.
- Segawa, A., Yamashina, S. and Murakami, M. (2002). Visualization of 'water secretion' by confocal microscopy in rat salivary glands: possible distinction of para- and transcellular pathway. *Eur. J. Morphol.* **40**, 241-246.
- Shachar-Hill, B. and Hill, A. E. (2002). Paracellular fluid transport by epithelia. *Int. Rev. Cytol.* **215**, 319-350.
- Spring, K. R. (1998). Routes and mechanism of fluid transport by epithelia. *Annu. Rev. Physiol.* **60**, 105-119.
- Van Itallie, C. M. and Anderson, J. M. (2006). Claudins and epithelial paracellular transport. *Annu. Rev. Physiol.* **68**, 403-429.
- Van Itallie, C. M., Fanning, A. S. and Anderson, J. M. (2003). Reversal of charge selectivity in cation or anion-selective epithelial lines by expression of different claudins. *Am. J. Physiol. Renal Physiol.* **285**, 1078-1084.
- Van Itallie, C. M., Rogan, S., Yu, A., Vidal, L. S., Holmes, J. and Anderson, J. M. (2006). Two splice variants of claudin-10 in the kidney create paracellular pores with different ion selectivities. *Am. J. Physiol. Renal Physiol.* **291**, 1288-1299.
- Van Itallie, C. M., Holmes, J., Bridges, A., Gookin, J. L., Coccato, M. R., Proctor, W., Colegio, O. R. and Anderson, J. M. (2008). The density of small tight junction pores varies among cell types and is increased by expression of claudin-2. *J. Cell Sci.* **121**, 298-305.
- Watson, C. J., Rowland, M. and Warhurst, G. (2001). Functional modeling of tight junctions in intestinal cell monolayers using polyethylene glycol oligomers. *Am. J. Physiol. Cell Physiol.* **281**, 388-397.
- Weinstein, A. M. and Stephenson, J. L. (1981a). Coupled water transport in standing gradient models of the lateral intercellular space. *Biophys. J.* **35**, 167-191.
- Weinstein, A. M. and Stephenson, J. L. (1981b). Models of coupled salt and water transport across leaky epithelia. *J. Membr. Biol.* **60**, 1-20.
- Yu, A. S., Cheng, M. H., Angelow, S., Günzel, D., Kanzawa, S. A., Schneeberger, E. E., Fromm, M. and Coalson, R. D. (2009). Molecular basis for cation selectivity in claudin-2-based paracellular pores: identification of an electrostatic interaction site. *J. Gen. Physiol.* **133**, 111-127.
- Zeissig, S., Bürgel, N., Günzel, D., Richter, J., Mankertz, J., Wahnschaffe, U., Kroesen, A. J., Zeitz, M., Fromm, M. and Schulzke, J. D. (2007). Changes in expression and distribution of claudin-2, -5 and -8 lead to discontinuous tight junctions and barrier dysfunction in active Crohn's disease. *Gut* **56**, 61-72.
- Zeuthen, T. (1995). Molecular mechanisms for passive and active transport of water. *Int. Rev. Cytol.* **160**, 99-161.
- Zeuthen, T., Meinild, A. K., Klaerke, D. A., Loo, D. D., Wright, E. M., Belhage, B. and Litman, T. (1997). Water transport by the Na⁺/glucose cotransporter under isotonic conditions. *Biol. Cell* **89**, 307-312.